Absorption of Beta Radiation
Radiation, Protection, Dosimetry and Detectors
SH2603

Christos Bellos, Miranda Carlström, Federico Pati

February 11, 2026

Contents

1 Introduction

In this laboratory report, the investigation of beta radiation and its absorption in materials will be discussed. Specifically, the energy spectrum of Cesium-137 and Strontium-90 will be analyzed using β and γ detectors to highlight their differences. Furthermore, the effect of beta radiation passing through increasing layers of aluminum foil will be examined to see how thickness impacts the beta electron spectrum. Finally, considering this attenuation, the range of the radiation will be evaluated.

2 Theory

2.1 Decay modes of Cs-137 and St-90

The analysis of Cesium-137 and Strontium-90 plays a significant role in nuclear safety, as they represent a large part of the radioactivity in nuclear waste and pose a considerable threat in the event of radiation release during accidents. Their stable isotopes are Cs-133 and Sr-88, respectively, and it is evident that our samples have more neutrons than the stable ones. Consequently, a β^- decay occurs in both, where a neutron is transformed into a proton, releasing an anti-electron neutrino and an electron, which constitutes the β^- radiation:

$$n \rightarrow p + e^- + \overline{\nu}_e \tag{1}$$

The energy spectrum associated with beta decay is continuous because, unlike α decay, three particles are involved, allowing momentum to be distributed in various ways. As a result, the energy of the emitted electron can vary widely, from the order of keV to MeV.

After β^- decay, the daughter nuclide may be created in an excited state. Excited nuclei will eventually decay to their ground state:

- By γ decay: the nuclei release energy by emitting a gamma photon, whose energy corresponds to the difference between the excited and ground states.
- By internal conversion: the nucleus transfers its excess energy to an electron in its surrounding atomic shell. This energy gain of the electron, typically located in the innermost shells, is in the form of kinetic energy and, if sufficient, the electron may escape from the atom. The vacancy left behind can then be filled by an outer electron, releasing energy in the form of X-rays.

According to the IAEA Live Chart of Nuclides [2], the decay scheme of Cs-137 is summarized in Figure 1. The most probable decay path, with a probability of 94.6%, is a β^- decay, releasing 0.512 MeV. The daughter nuclide, Barium-137m, is still unstable and predominantly releases its energy by emitting a gamma photon. Alternatively, in 5.4% of cases, Cesium releases all its energy in a single β^- decay to Ba-137 in its ground state.

On the other hand, Strontium-90 undergoes a single β^- decay, releasing 0.546 MeV. Its daughter, 90^{Y}, initiates a chain of further radionuclides undergoing β^- decay.

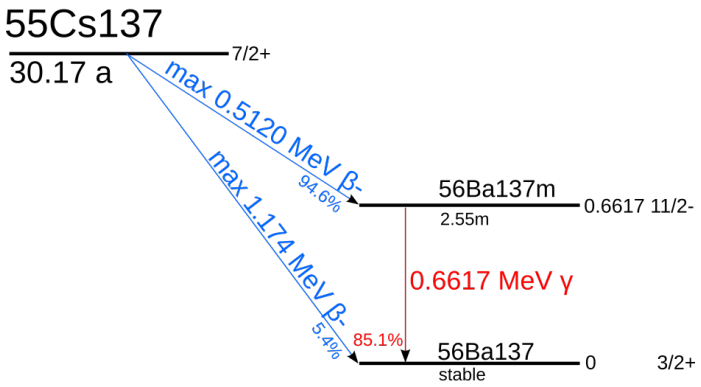

Figure 1: Cesium-137 decay.[4]

2.2 Interaction of beta radiation with matter

Regarding interactions with matter, electrons lose their kinetic energy by interacting with the atomic electrons of the material. However, due to their small mass, they are easily affected by the electromagnetic field of the nuclei, causing changes in their velocity vectors and generating X-rays (Bremsstrahlung radiation). At energies below a few MeV, the loss due to collisions dominates, and the stopping power can be expressed by the Bethe-Bloch formula:

$$-\frac{dE}{dx} = 2\pi N_a r_e^2 m_e c^2 \rho \frac{Z}{A}\frac{1}{\beta^2}\left[\ln\frac{\tau^2(\tau+2)}{2(I/m_e c^2)^2} + F(\tau) - \delta - 2\frac{C}{Z}\right] \tag{2}$$

where Z, A, and ρ are the atomic number, atomic weight, and mass density of the material, respectively. N_a is Avogadro's number, m_e is the electron mass, and I is the mean excitation energy of the atomic electrons in the stopping material. τ is the kinetic energy of the electron projectile, and the function $F(\tau)$ differs for electrons and positrons.

The stopping power due to Bremsstrahlung becomes increasingly relevant at higher energies, and its expression is:

$$-\frac{dE}{dx} = NE_0\Phi_{\text{rad}} \tag{3}$$

where E_0 is the total initial electron energy, Φ_{rad} is a function that depends only on the material, and N is the number of atoms per unit volume in the material.[1]

2.3 Scintillators

A NaI scintillator works by converting incoming radiation, typically gamma rays, into visible light, which can then be detected and analyzed. These detectors consist of scintillating materials (in this case, an NaI crystal) that emit light when hit by ionizing radiation. Specifically, when high-energy gamma rays or X-rays interact with the crystal, they transfer energy to the electrons within the material, meaning that the atomic electrons absorb the gamma radiation and become excited. The electrons move to higher energy states and eventually

return to their ground states by emitting photons in the visible light range. The energy of these photons is equal to the difference between the two energy states of the atom. The intensity of this scintillation light is directly proportional to the energy of the incoming radiation.

When the NaI scintillator is used to measure beta radiation, the detection process changes since beta particles interact with the material differently than photons. Beta particles are already charged, so they interact directly with the atoms in the NaI crystal as they travel through, causing ionization and excitation. As they do so, beta particles deposit their energy continuously along their path, and this deposition depends on their initial kinetic energy. As a result, the beta spectrum is continuous, in contrast to the sharp peaks observed in gamma detectors.

The direct ionization and excitation of the atoms of the scintillator material will also lead to visible light emission as the excited atoms return to their lower energy states.

The visible light (photons) produced in each case travels through a tube, with a window covered by a thin layer of material known as the photocathode. At this point, the photoelectric effect occurs, generating primary electrons. These electrons are then directed inside the photomultiplier tube, which contains a series of electrodes at progressively higher electric potentials. Consequently, the electrons are accelerated and multiplied, eventually leading to the production of an electron pulse. This pulse is amplified and collected by the system, where it is analyzed using the Tukan software.

3 Experimental Setup

The experimental setup consists of two scintillation detectors connected to a computer equipped with Tukan analysis software, which is used to detect gamma and beta radiation.

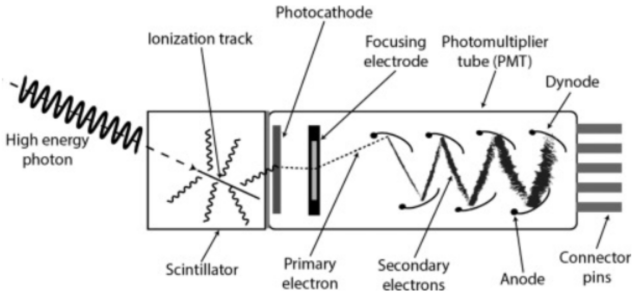

Figure 2: Detector operation

3.1 Method

Firstly, the energy spectrum of Cs-137 was measured using the gamma detector. The open Cs-137 source was placed under the detector, and the spectrum was recorded. The process was repeated with St-90 with the aim of comparing the

spectra and analyze the processes involved in each. Next, the measurements were repeated using the beta detector.

Using the known energy of internal conversion peak for Ba-137, the beta spectrum for Cs-137 could be calibrated. This energy is the full energy of Ba-137 in its excited state, minus the binding energy of the K-electron:

$$E = 661.7keV - 37.4keV = 624.3keV \tag{4}$$

To study the absorption of beta radiation, thin layers of aluminum were then inserted between the Cs-137 source and the beta detector. The energy of the internal conversion peak present in the spectrum was measured for increasing thickness of aluminium shielding. By linearly extrapolating the relationship between the energy of the peak and aluminium thickness, the range of the beta particles at set energies could be determined. These values were then fitted to a function $R(E) = a \cdot E^b$.

4 Results

4.1 Beta and gamma spectra

The beta emission spectrum of St-90 is depicted in figure 3. As expected, we see a continuous spectrum of beta particle energies. However, the spectrum does not fit a pure Fermi distribution since Y-90 also undergoes beta decay. Therefore, the spectrum is a superposition of the Fermi distributions of the St-90 and Y-90 electrons. The individual distributions have been sketched approximately with dashed lines in figure 4.

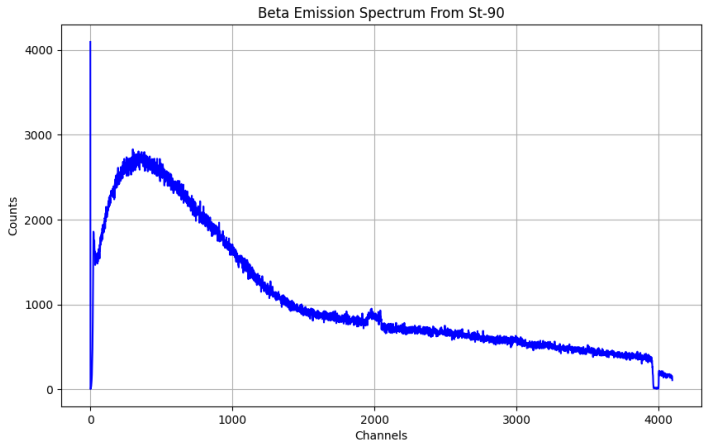

Figure 3: Beta emission spectrum from pure beta emitter St-90 and its daughter nuclide Y-90.

Despite St-90 being a pure beta emitter, the NaI scintillator still detected photons from this source in a continuous spectrum, see figure 5. This is Bremsstrahlung radiation; the electrons emitted from St-90 and Y-90 slow down when entering and interacting with the aluminium cover around the scintillator by emitting

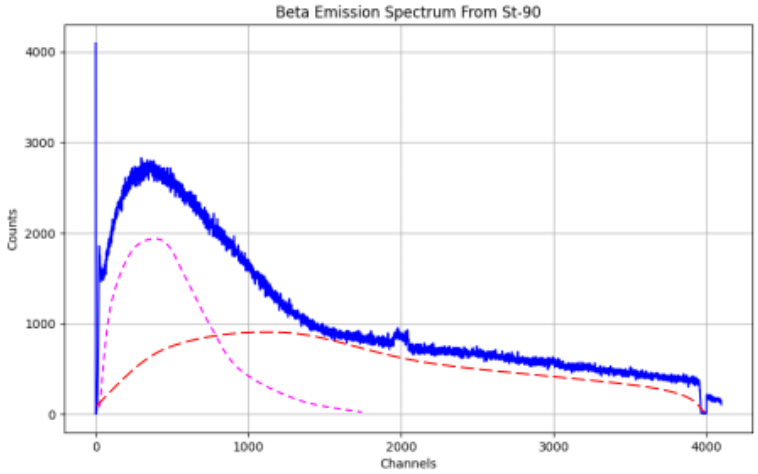

Figure 4: Beta emission spectrum from St-90 with dashed lines sketching the individual Fermi distributions for St-90 (pink) and Y-90 (orange).

photons. Note that while the energy spectrum of these photons overlap with that of gamma radiation, they do not count as such since they were not produced through the de-excitation of an atomic nucleus.

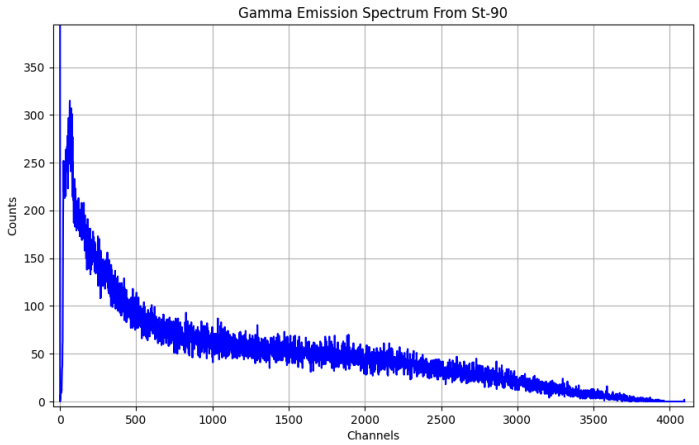

Figure 5: Spectrum obtained from St-90 sample by gamma detector.

By comparison, Cs-137 is not a pure beta emitter since Ba-137 can either gamma decay or undergo internal conversion. The contributions of these processes dominate the photon energy spectrum for the Cs-137 sample, see figure 8, and therefore it is not possible to identify the contribution of the Bremstralung radiation in the aluminium cover in the spectrum.

The beta emission spectrum for Cs-137 is also continuous, with two rounded peaks, see figure 7. The first peak, which ís also the highest, matches the peak

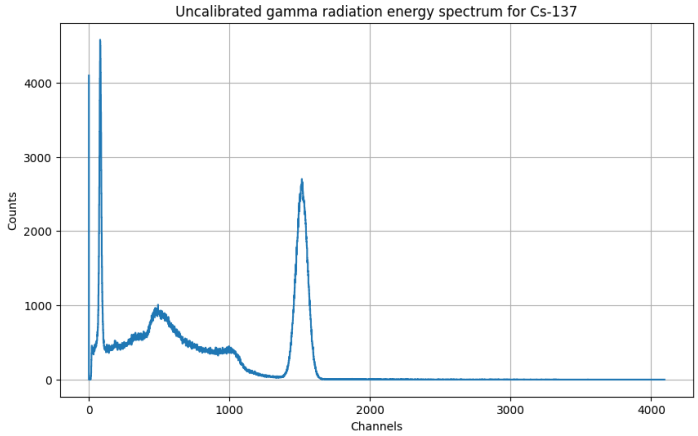

Figure 6: Spectrum obtained from Cs-137 sample by gamma detector.

of the Fermi distribution of Cs-137 beta decay into Ba-137. However, the second peak does not hail from the beta emission at all. Instead, these electrons stem from the internal conversion of the excited Ba-137 nucleus. As such, the energy of the internal conversion peak can be determined to correspond to 624.3 keV. This is used to calibrate the energy spectrum, along with assigning zero energy to the first channel.

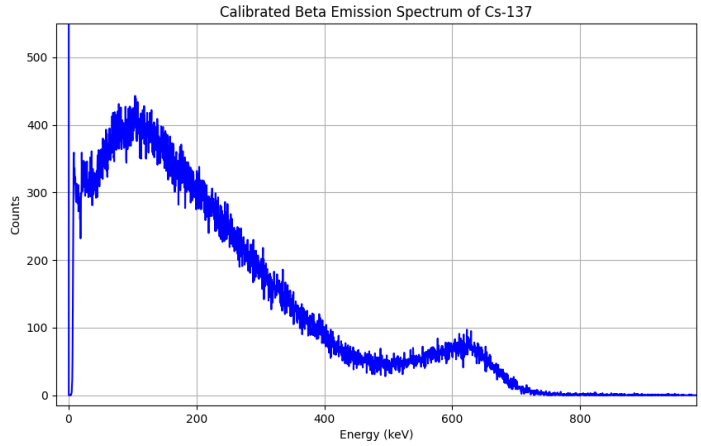

Figure 7: Calibrated beta emission spectrum of Cs-137. The internal conversion peak of Ba-137 is situated at 624.3 keV.

4.2 Electron range in aluminium

Layers of aluminum foil were inserted between the Cs-137 sample and the detector. The resulting shift in the registered energy of the internal conversion peak

of Ba-137 is displayed in Figure 8. Since the emitted electrons during internal conversion have a known energy of 624.3 keV, the energy of the peak recorded for a given aluminum shield thickness reveals the energy loss of the electrons as they travel through that thickness.

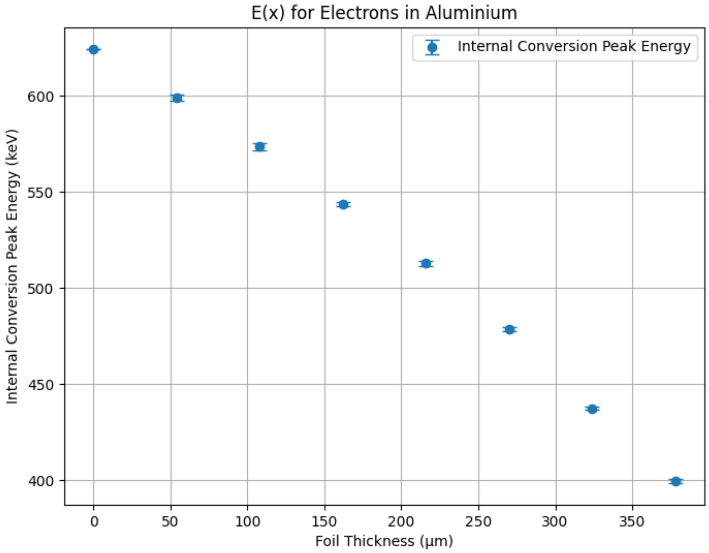

Figure 8: The decrease in electron energy as a function of distance travelled inside aluminium.

The range R of the electrons is defined as the distance x travelled inside of a medium for which $E(x) = 0$. It can be determined by linearly extrapolating of the energies in figure 8 in order to find the intersection with the x-axis.

Naturally, the range R depends on the initial energy E. Here, a piecewise relationship in the form $R(E) = a \cdot E^b$ is assumed, where a and b are coefficients that must be determined. Usually, determining these coefficients requires measuring the range at several known electron energies.

However, instead of conducting multiple experiments with different sources to achieve various known energies, the energy of the internal conversion peak at each thickness of aluminum foil provides a known electron source that subsequently travels through the remaining layers. Therefore, from n data points of peak energy at different thicknesses, $n - 1$ range-energy data points can be extrapolated. This allows for establishing the range-energy relationship using just a single experiment.

Figure 10 shows the measured ranges along with the fitted function $R = a \cdot E^b$, where $a = 0.5850$ and $b = 1.431$. For reference, NIST values for electron range are also plotted, and significant agreement between the measured values and the reference values can be observed.

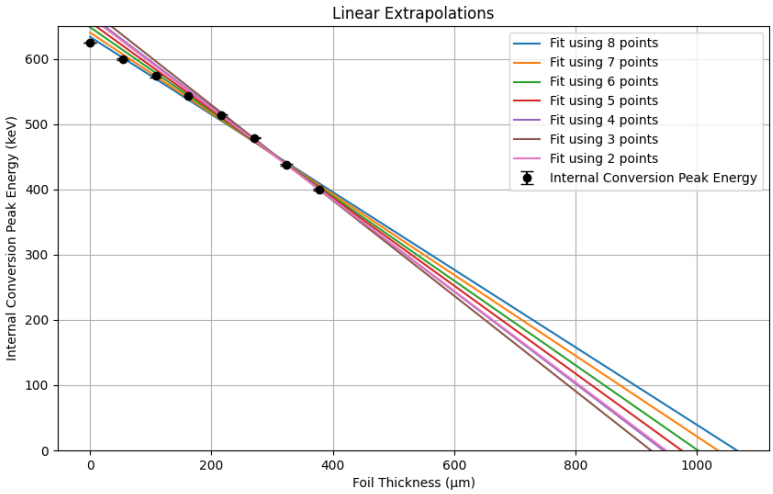

Figure 9: Linear extrapolations of $E(x)$ using a decreasing number of data points. The horizontal distance from the data point of energy E to the extrapolation's intersection with the x-axis provides the range of an electron at that energy, $R(E)$.

5 Conclusion

In conclusion, this experiment demonstrated the interaction of beta radiation with matter by investigating the absorption and energy loss of beta particles as they traveled through varying thicknesses of aluminum. The known energy of the internal conversion peak of Ba-137 allowed for calibration of the electron energy spectrum emitted by Cs-137. By measuring the shift in energy of this peak with increasing aluminum thickness, the range of the electrons was determined through linear extrapolation. The experimental data provided multiple range-energy points, which were then fitted to a function $R(E) = a \cdot E^b$. The coefficients found, $a = 0.5850$ and $b = 1.431$, produced a relationship that aligned closely with reference values from NIST. This confirms that the range of beta particles in aluminum can be effectively measured and modeled using this method.

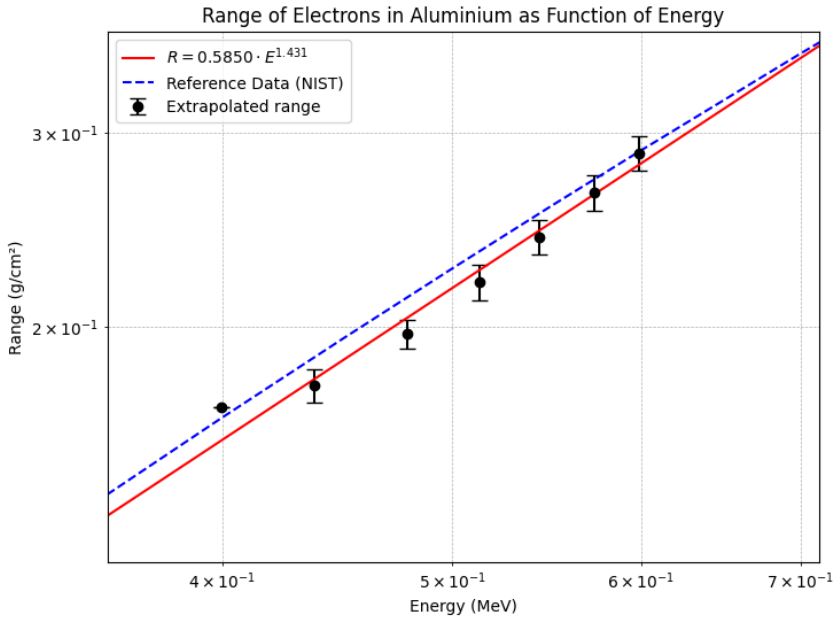

Figure 10: Data points for range as function of electron energy along with fitted function $R = 0.5850 \cdot E^{1.431}$ (red). Known values of electron range as a function of energy are plotted for reference (blue) [3].

References

[1] Torbjörn Bäck. Radiation protection, dosimetry, and detectors compendium, September 5, 2023 (version 1.9).

[2] IAEA. Livechart - Table of Nuclides - Nuclear structure and decay data — www-nds.iaea.org. https://www-nds.iaea.org/relnsd/vcharthtml/VChartHTML.html. [Accessed 2024-09-24].

[3] NIST. Estar - stopping power and range tables for electrons — www-nds.iaea.org. https://physics.nist.gov/cgi-bin/Star/e$_t$*able.pl*.

[4] Ervin B. Podgorsak. *Radiation Physics for Medical Physicists*. Springer Berlin Heidelberg, 2010.